Journal of Fertilization: In vitro - IVF-Worldwide, Reproductive Medicine, Genetics & Stem Cell Biology

Malecki and Malecki, J Fert In Vitro 2012, 2:3
DOI: 10.4172/2165-7491.1000108

Research Article

Routing of Biomolecules and Transgenes' Vectors in Nuclei of Oocytes

Marek Malecki[1,2]* and Bianca Malecki[2,3]

[1]*Western University of Health Sciences (WUHS), Pomona, CA, USA*
[2]*Phoenix Biomolecular Engineering Foundation (PBMEF), San Francisco, CA, USA*
[3]*Jagiellonian University (JU), Krakow, PL, EU*

Abstract

The molecular architecture of Nuclear Pore Complexes (NPCs), as well as the import and export of molecules through them, has been intensively studied in a variety of cells, including oocytes. However, the structures and mechanisms, involved in the transport of molecules beyond the NPCs, remained unclear, until now. The specific aim of this work was, therefore, to determine, if there exist any intranuclear structures *in continuum* with the NPCs. This information could help in explaining the mechanisms, which propel the distribution of biomolecules and vectors inside the cell nuclei.

To attain this aim, we used rapid cryo-immobilization to capture molecular processes of living cells with millisecond resolution. We pursued molecular imaging, including electron energy loss spectroscopy and energy dispersive x-ray spectroscopy, to reveal structures with nanometer spatial resolution. We also bioengineered single chain variable fragments to track biomolecules and transgenes' constructs.

Herein, we reveal the Nuclear Routing Networks (NRNs) in the oocytes of *Xenopus laevis*. The NRNs originate at and extend from the tops of intranuclear baskets of the NPCs to interconnect them, while creating a complex, intra-nuclear, three-dimensional architecture. The NRNs guide the export of both tRNA, as well as the Nuclear Export Signal (NES) equipped vectors, from the nuclei. Moreover, the NRNs guide the import of both nucleoplasmin, as well as the Nuclear Localization Signals (NLS) modified transgenes' vectors, into the nuclei. The vectors equipped with these NLS and NES shuttle back and forth through the NPCs and NRNs.

To summarize, we reveal the NRN, which functions as the guided distribution system in the *Xenopus laevis* oocytes' nuclei. We further proceed with the identification of its molecular components.

Abbreviations: NE: Nuclear Envelope, NPC: Nuclear Pore Complex, NRN: Nuclear Routing Network, Np: Nucleoplasmin, H: histone, tRNA: Transfer Ribonucleic Acid, mRNA: Messenger Ribonucleic Acid, NLS: Nuclear Localization Signal, NES: Nuclear Export Signal, gDNA: Genomic DNA, ISH: In Situ Hybridization, scFv: Single Chain Variable Fragments, NGS: Next Generation Sequencing, NMR: Nuclear Magnetic Resonance, SPM: Surface Plasmon Resonance, EELS: Electron Energy Loss Spectroscopy, EDXS: Energy Dispersive X-Ray Spectroscopy

Introduction

Genomic DNA is sealed within the nuclear envelopes (NEs) in all eukaryotic cells. Entry of molecules into, as well as exit from the nuclei occur exclusively through nuclear pore complexes (NPCs). Therefore, the most fundamental processes of living cells, in both health and diseases, all involve transport of the molecules through the NPCs [1-9].

At present, numerous studies are conducted about the transport of molecules through nuclear pore complexes (NPCs) and their molecular architecture, in a variety of cells including oocytes [10-11]. In addition to insight for general knowledge, such studies have also the strong clinical relevance. Recent developments in molecular profiling facilitate identification of genetic errors with high accuracy [12-15]. Some genetic errors result in disorders responsible for infertility, miscarriages, and for almost half of the infant and neonatal deaths. Still others are responsible for high susceptibility to development of diseases later in life, e.g., increased risks of cancers in carriers of inherited BRCA1 mutations [16-18]. Pre implantation genetic testing greatly advanced the success of *in vitro* fertilization (IVF) by guiding the selection of healthy embryos [19-20]. Furthermore, *in uterus*, amniotic and chorionic, genetic testing and USG, help to identify genetic disorders early on in development [21-25]. While the test results, indicative of genetic disorders, may lead some women to terminate pregnancies, genetic engineering aimed at correcting these errors, and thus preventing those genetic disorders from developing, is currently a futuristic temptation. Nevertheless, development of some mutations involves passing of mutagens through the NPCs and reaching the gDNA, e.g., HIV leading to the congenital AIDS. Engineering viral blockers of the NPC docking sites for importinβ /karyopherinβ clusters could be a preventive step. While retroviruses used in gene therapy trials exert their therapeutic effects upon genomic integration, but can also present a threat of the virus-induced insertional mutagenesis in genes of oocytes. Intelligent biomolecular engineering of the transgenes' vectors, with the precisely defined transporting steps, should be one of the safeguards [26-28].

However, the structures and mechanisms involved in the transport of molecules beyond the NPCs remained unclear until now. Interestingly, in various published images of the NEs, there existed apparent, short, thin filaments radiating out from the inner ring of the NPCs towards the nuclear interior and from the cytoplasmic ring towards the cytoplasm [29-39]. The relationships of these short filaments to the NPCs and their ultrastructural organization indicated structures entirely different from lamins or matrices [38,39]. In addition, a few publications on nucleo-cytoplasmic transport contained observations, that viruses, gold-tagged molecules, or transcripts were often aligned in the nuclei into single file tracks; however the authors neither revealed any supporting structures, nor interpreted underlying mechanisms [40-44].

***Corresponding author:** Marek Malecki, MD, PhD, Associate Professor of Genetics, Genomics, and Gene Therapy, Western University of Health Sciences (WUHS), Pomona, CA, USA, on leave at the UW, Tel: 4157134370; E-mail: MM@PBMEF.ORG

Received March 22, 2012; **Accepted** April 20, 2012; **Published** April 30, 2012

Citation: Malecki M, Malecki B (2012) Routing of Biomolecules and Transgenes' Vectors in Nuclei of Oocytes. J Fert In Vitro 2:108. doi:10.4172/2165-7491.1000108

Nevertheless, rapid trafficking of histones had to be supported by very efficient transport system [45]. Studies suggested compartmental organization of chromatin and patterns of expression contingent upon the distribution of genes in relation to the NE [45-49]. Furthermore, molecules contributing to the buildup of the NPCs were shown as having DNA binding properties [50].

The ultimate goal of our work is genomic nanosurgery, which would include guided trafficking of the vectors to the defined loci on chromosomes for: (1) repairing of the mutated genes, (2) safeguarding gDNA against induction of mutations, or/and (3) inserting genes promoting resistance against diseases [51]. Precise knowledge of the functional structures involved in the nuclear transport processes is essential. The specific aim of this work was, therefore, to determine, if there are any intranuclear structures *in continuum* with the NPCs. In this regard, our report helps in explaining mechanisms, which propel transport of molecules, of importance for biology and medicine, inside the nuclei of oocytes.

Materials and Methods

Oocytes of *Xenopus laevis*

Mature *Xenopus laevis* oocytes were used in this study as the well established model of nucleo-cytoplasmic transport. They were gifts from Dr J. Dahlberg, Dr E. Lund of UW Madison, Dr M. Kloc, UT Dallas, and Dr D. Forbes, UC San Diego. The oocytes were defolliculated and maintained in amphibian Ringer's solution. The nuclei were isolated in the low salt buffer (LSB: 0.5mM $MgC1_2$, 1mM KCI, 0.1mM ATP, 10 mM Hepes, pH 7.4) by tearing the oocyte surface at the pigment border with forceps. They were then cleaned of yolk with dissecting needles and attached to glass, gold, or carbon chips treated with silane and gutaraldehyde [30]. Live recording was performed using a CCD camera (C5985, Hamamatsu, Japan) under and MetaMorph imaging software (Universal Imaging, Corporation, West Chester, PA).

Isolation of nuclear envelopes

The oocyte nuclei contained a contractile gel due to the presence of actomyosin. In order to see the structures on the inside of the NE, the nuclei were rinsed with Macgregor's 5:1 buffer (10 mM HEPES, 83mM KCI, 17 mM NaCI, 0.5 mM $MgC1_2$, 0.1mM ATP, pH 7.4) and opened with microneedles. For studies of the active transport of the vectors, the buffers were supplemented with 0.3 mM apyrase or maintained at 4 deg. C. Nuclear envelopes (NE) remained attached to the sticky carriers during all procedures that followed [32]. The NE samples were either chemically fixed or rapidly cryo-immobilized.

Nucleoplasmin, histone, transfer RNA, messenger RNA, NLS and NES equipped vectors

Nucleoplasmin, a 165kDa karyophilic protein known to be imported through the NPCs, was prepared according to the classical protocol [52-53]. Briefly, oocytes were rinsed in Ca-free Ringer's solution containing phenylmethylsulfonyl fluoride, homogenized, cleared by centrifugation, extracted with 1,1,2-trichlorotritluoroethane. DEAE-cellulose and phenyl sepharose column chromatography were followed by ammonium sulfate extraction and dialysis against 50 mM Tris-HCl. The purity quality control was performed on the native gel with the gold enhanced silver staining. Human 150kDa IgG served as the control [63]. The biomolecules were modified with biotin or digoxigenin for detection with the scFv coordinating Gd, Eu, Au, Tb, Er, or Ag atoms for NMR, SPR, FM, EDXS, and EELS, as described [63].

Transfer RNA, known to be exported through the NPCs, was prepared according to the classical protocol [54-56]. The templates for transcription tRNAi Met were generated by linearization of plasmids and in vitro transcription with v T7RNApolymerase (Promega) as uncapped RNA. Total RNA served as the control. Transcription mix included biotin labeled analog of guanosine triphosphate (GTP) (Biotin-11-GTP) (Perkin Elmer) to facilitate detection with chelating scFv [63].

The vectors were engineered as organo-metallic clusters containing multiple, hetero-functional domains as recently described [14]: (i) single chain variable fragment antibodies (scFv) targeting biotin or digoxigenin – anchoring the plasmid DNA having incorporated dNTPS modified with biotin digoxigenin; (ii) scFvs targeting dsDNA – holding dsDNA; (iii) metal binding domains; (iv) nuclear localization signals (NLS); (v) nuclear export signals (NES). The coding sequences for the anti-digoxigenin and anti-biotin scFv were amplified by polymerase chain reaction using the mix of the plasmid DNA, synthesized primers, dNTPs, and Taq DNA polymerase (Hoffmann–La Roche, Basel, Switzerland) using the Robocycler (Stratagene, San Diego, CA) from the constructs described earlier [14]. The coding sequences for the anti-dsDNA scFvs were generated from the blood as described earlier. Briefly, fresh blood was received from the patients suffering from Lupus erythomatosus with the Institutional Review Board (IRB) approval and with the Informed Consent Forms (ICF) signed. The B cells were isolated using the superparamagnetic scFvs targeting CD19 and CD20. The total mRNA was isolated using Trizol reagent (Molecular Research Center, Inc. Cincinnati, OH). The cDNA was generated using random hexamers (Intergrated DNA Technologies, Coralville, IA) and reverse transcriptase (Promega, Madison, WI). The cDNA quality was tested by the polymerase chain reaction (PCR) of beta actin and GAPDH as reference genes with the commercially available primers (ABI, Foster City, CA). For amplification of variable fragments, the primers sets were designed using the Kabat database. They were synthesized on 380A DNA Synthesizer (ABI, Foster City, VA). The closed, circular, dsDNA plasmid constructs coding for the scFv targeting catalase and superoxide dismutase were prepared and tested for their integrity during the trafficking as recently described [14,27].

The coding sequence for the NLS – PKKKRKV was amplified from the SV40 Large T antigen plasmid (ATCC, Manassas, VA). The coding sequence for the NES – LPPLERLTL was amplified from the HIV Rev plasmid (ATCC, Manassas, MD) [59,60]. The scFvs without NES and NLS served as the controls. The coding sequences were cloned into the plasmid vector and expressed in myelomas (ATCC, Manassas, VA). Alternatively, they were synthesized (ABI, Foster City, CA).

Microinjections

Xenopus laevis oocytes were maintained in amphibian Ringer's solution. Just prior to the microinjections, the oocytes were spun down at 650g to position the nucleus just below the plasma membrane near the animal pole. This facilitated the intranuclear microinjections. This also assured the perinuclear microinjections close to the nuclear envelope, but without mistakenly injecting the nuclei. Then, intra-cytoplasmic and intra-nuclear microinjections were conducted using glass micropipettes (10 micrometer mouth diameter) mounted into micromanipulator (Narishige, Tokyo, Japan) on an inverted microscope (Nikon, Tokyo, Japan or Zeiss, Oberkochen, Germany) according to established procedures. Exactly 50 nL volumes of solutions containing non-viral transgenes' vectors or biomolecules were injected by pressure controlled pulses. At different time intervals, the whole oocytes were cryo-immobilized in the high-pressure freezing machine (HPM10, Balzers, Lichtenstein). Subsequently, the concentrations of the transgenes in dif-

ferent organelles of the oocytes were measured by means of elemental analysis with EDXS or EELS [63].

Cryo-immobilization

At the completion of the experiment, the cells were cryo-immobilized within 10 ms down to –196°C at 2000 atm within the pressure chamber of the high pressure freezing machine HPM10 (Bal-Tec, Liechtenstein). Alternatively, if the nuclear envelopes were isolated and attached to the chips, then they were cryo-immobilized within liquid pentane using the plunge freezer [30]. All the samples were stored in liquid nitrogen until further processing by freeze-substitution and embedding for sectioning FSD010 (Bal-Tec, Liechtenstein) or freeze-fractured and freeze-dried BAF 060 (Bal-Tec, Liechtenstein).

Chemical fixation

Isolated *Xenopus laevis* oocyte nuclei attached to the chips were fixed in 1% glutaraldehyde and 0.2 % tannic acid in the LSB. This was followed by post-fixing in 1% osmium tetroxide in the LSB. They were cryo-immobilized by plunge freezing and stored in liquid nitrogen. After freeze-substitution with acetone on FSD010 (Bal-Tec, Liechtenstein), the preparations were embedded in epon 812 (Ladd, Williston, VT) and sectioned. Alternatively, the samples were dehydrated in ethanol, dried in critical point of CO_2, and cryo-sputter-coated with Pt/C on BAF060 (Bal-Tec, Liechtenstein) [30].

Molecular imaging and elemental analysis

The field emission, scanning transmission, electron microscope FESTEM HB501 (Vacuum Generators, Kirkland, WA) was equipped with the energy dispersive x-ray spectrometer (EDXS) (Noran, Middleton, WI) and the post-column electron energy loss spectrometer (EELS) (Gatan, Pleasanton, CA). The cryo-energy filtering transmission electron microscope 912 Omega was equipped with the in-column, (Zeiss, Oberkochen, Germany). The images were acquired using the ccd camera operating under the image acquisition and processing software (SIS, Herzogenrath, Germany or Emispec Systems, Tempe, AZ). The field-emission scanning electron microscopes S3400 was equipped with the EDXS (Hitachi Tokyo, Japan) and SEM1530 (Zeiss, Oberkochen, Germany) was equipped with EDXS (Noran, Middleton, WI). For stereo-viewing, the in-register pairs of images were acquired electronically with +/- 6 degrees tilt of the stage. The control elemental spectra were acquired on the standards from the National Institute of Standards and Technology (NIST, Gaithersburg, MD). The concentrations of the vectors at different compartments were determined using EDXS and EELS spectral mapping. All the vectors contained the domains chelating Gd, Tb, Eu, Au, Er or Pt. EDXS and/or EELS elemental spectra were acquired for every single pixel of the imaged area to create the elemental data stack. From this stack, the map of the selected element was extracted to create the map of this element's distribution with the element's concentration determined. The overall oocyte ultrastructure was revealed using EELS at zero energy loss. The elemental maps of the exogenous atoms (e.g., Gd atoms chelated into the vectors) were overlapped over the ultrastructural map of the oocyte. This way the concentrations of the vectors within the oocytes' compartments were determined. For the overviews of the cell architecture either high voltage transmission electron microscope operated at 1 MeV (AEI, EM7) or energy filtering transmission electron microscope operated at 120 keV at zero energy loss (LEO912) were used.

Results

Figure 1 illustrates the work-flow of the project. The oocytes were de-folliculated. (a) They were spun down to move the nuclei to the poles, in order to facilitate intra- or peri-nuclear microinjections of the vectors. That was followed by rapid cryo-immobilization, processing, and determination of the transgenes' concentration with the aid of the EDXS and EELS. (b) Alternatively, the nuclei were isolated. (c) Thereafter, the nuclei were opened to remove nucleoplasm. (d) The nuclear envelopes, attached to the carriers, were cryo-immobilized and processed for (e) molecular imaging and elemental analysis with the aid of the EDXS or EELS.

The intra-nuclear surface of the nuclear envelope (NE) was exposed by gentle removing chromatin gel, which followed by chemical fixation, critical point drying, and cryo-sputter-coating. It was revealed in the field emission scanning electron microscope (FESEM), as illustrated in the figure 2. In the field of view, there are present numerous "baskets" of the nuclear pore complexes (NPC), which protrude from the nuclear envelope. They are marked with the red arrows pointing toward the entries into the nucleus. Bundles of 6 nm thin filaments project from the tops of most of the NPC "baskets". The bundled filaments create empty nanotubes. They project into the nucleus' interior. These bundles extend for distances from 2 micrometers to more than 10 micrometers in lengths. Short and long stretches of the filamentous bundles interconnect with each other to form nuclear networks. In a few cases, attached fibers have all broke off the "baskets", thus revealing the top rings only. At all distal ends of the eight fibers (projecting from the 145 nm diameter, nuclear ring of the NPCs) there are the 10 nm in diameter spheres. These spheres attach to each other to form the "necklace-like" rings - as if they would be holding together the bundles of filaments. These rings are distributed along the filamentous bundles with the regular periodicity of approximately 50 nm. They are pointed with the red arrow-heads. Lamins networks are marked with the red stars. They seem to create a stabilizing base for the NPCs inserted in their nets.

Organization of the filaments projecting from the NPCs was also revealed by cryo-electron energy loss spectroscopy at the zero-loss energy setting as shown in the figure 3a. The oocytes were prepared by rapid cryo-immobilization, freeze-substitution, and sectioning of 250 nm sections. This technique of the specimen preparation was entirely different from that used for the FESEM preparations. Yet, the bundles of filaments project from the tops of the NPCs on the identical way as the ones shown in the figure 2. They also have the "necklace-like"

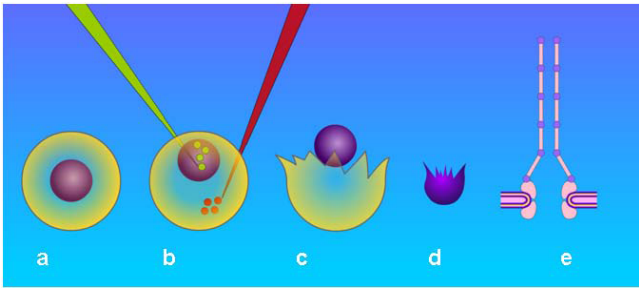

Work-flow of the oocyte's Nuclear Routing Network (NRN) preparation and graphic summary of the project

Figure 1: The Xenopus laevis oocytes were defolliculated and stored (a). After spinning, which aimed at moving the nucleus to the pole, the transgenes vectors and biomolecules, equipped with the NLS and NES, were microinjected into the cytoplasmic or intra-nuclear compartments of oocytes (b). Some of the microinjected oocytes were cryo-immobilized for the trafficking and molecular imaging studies. The nuclei from other oocytes were isolated (c). The nuclei were attached to carriers and wide opened to release nucleoplasm (d). The nuclear envelopes with the retained NPCs and NRNs were available for molecular imaging (e).

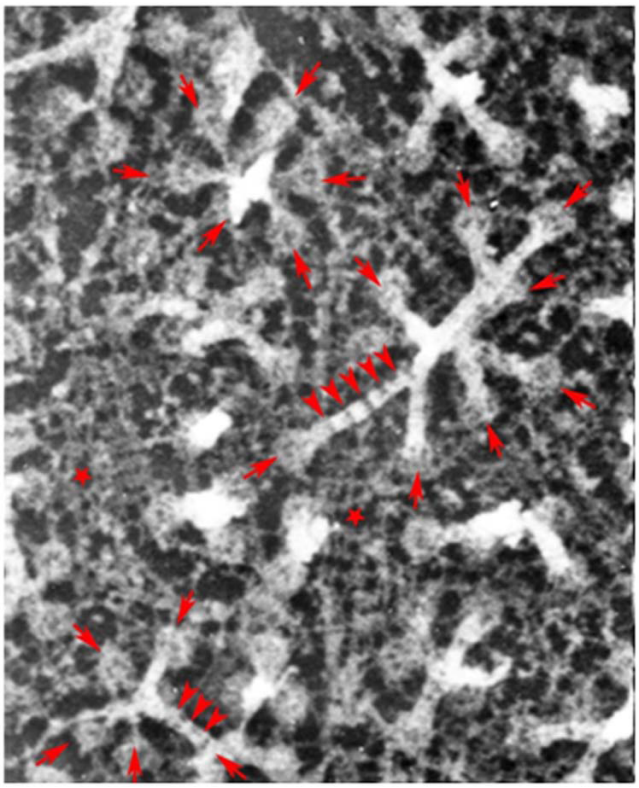

Three-dimensional architecture of the Nuclear Routing Network (NRN) revealed by Field Emission Scanning Electron Microscopy (FESEM) of the nuclear envelope whole-mounts.

Figure 2: The intra-nuclear surface of the NE was exposed by gentle dissolving chromatin gel. The nuclear envelope was isolated in LSB, attached to a modified (sticky), glass chip, extracted with 0.1% Triton X-100 and fixed with 1% glutaraldehyde in LSB, postfixed with 1% aqueous osmium tetroxide, critical point dried, followed by cryo-sputter coating with Pt. It was imaged in the FESEM operated at 1.5kV. Entries into the nucleus through the NPCs are pointed with the red arrows. The NRNs project from the tops of the NPCs and show regular 50 nm periodicities pointed with red arrow-heads. The NRNs inter-connect to form a network. Lamins are marked with red stars. Horizontal field width 1820 nm.

rings distributed along their lengths with the periodicities identical to those revealed above. They are also pointed with the red arrow-heads. Although, the NPCs are buried within the thick sections, the baskets of the NPCs are clearly seen. The red arrows point to the entries into the nucleus through the NPCs. Alternatively, the oocytes were embedded through the conventional methods and imaged with the high voltage transmission electron microscope as shown in the figure 3b.

Yet, the third, entirely different method of the oocytes' preparation for molecular imaging, shown in the figure 4, resulted in the identical appearance of the filamentous networks projecting from the NPCs as those illustrated in the figures 2,3. In this case, the nuclear envelopes were rapidly cryo-immobilized, embedded, cut into the serial 250nm thick sections, and de-embedded. The NPCs with the associated structures were revealed in the FESEM. In this image, there is the NPC basket with its smaller, intra-nuclear ring pointed with the white arrow. The NPC has larger ring at the bottom, at the level of the intra-nuclear surface of the nuclear envelope, which holds the NPC basket. From the top of this NPC basket, project bundles of filaments. Along their lengths and with the regular 50nm periodicity, there are the necklace-like rings consisting of the 10 nm in diameters spheres. These bundles form inside-hollow nano-tubes.

The data acquired with these three different methods revealed the networks of the filamentous bundles held together by small spheres assembled into the necklace-like rings. Summarizing the data from the figure 2-4, the bundled filaments, create nanotubes interconnected into the three-dimensional networks. These data were integrated into the model presented in the figure 5. This structure has all of the characteristics expected from networks routing molecules throughout the nucleus. Therefore, we hypothesized that it be the nuclear routing network (NRN). To test this hypothesis, functional studies of these newly discovered networks followed.

The vectors were bioengineered to carry the closed, circular dsDNA

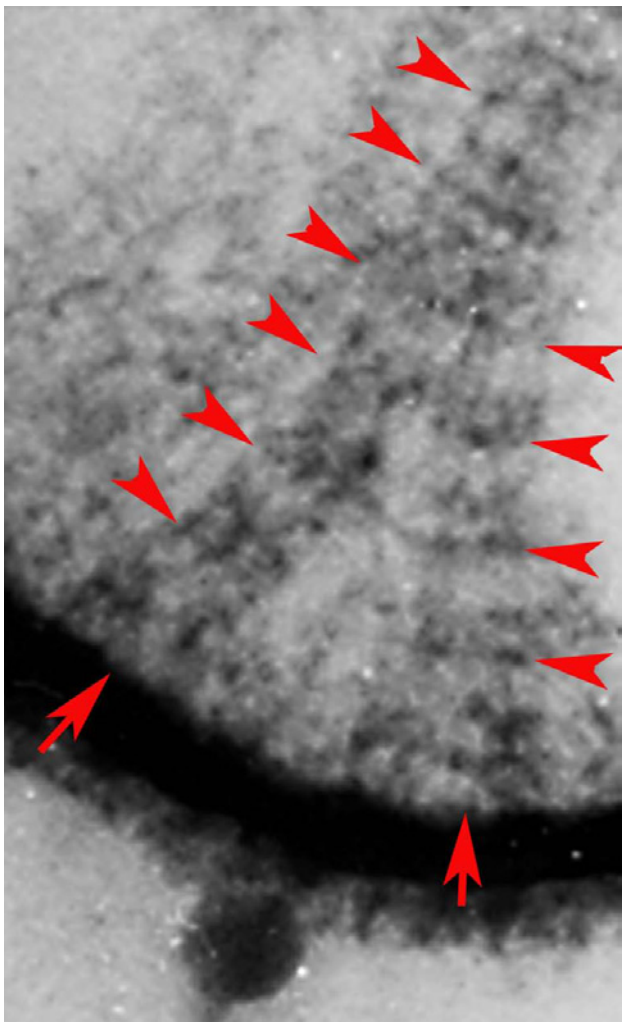

Three-dimensional architecture of the nuclear routing networks (NRNs) revealed by Electron Energy Loss Spectroscopy (EELS) in 250 nm thick sections

Figure 3a: This oocyte was rapidly cryo-immobilized, after perinuclear microinjection with the NLS carrying transgenes. It was further processed by freeze-substitution, embedding, and cutting 250 nm thick sections. The image was acquired at zero loss setting of the energy loss energy spectrometer (EELS). The arrows point to the entries into the nucleus through the NPCs. Bundles of long thin filaments stretch from tops of NPC into the nuclear interior to form the NRNs. Along their long axes, there are "necklace-like "structures periodically distributed along the filaments. The heavily electron-dense dots suggest the vectors trafficking through the NRNs. Horizontal field width 450 nm.

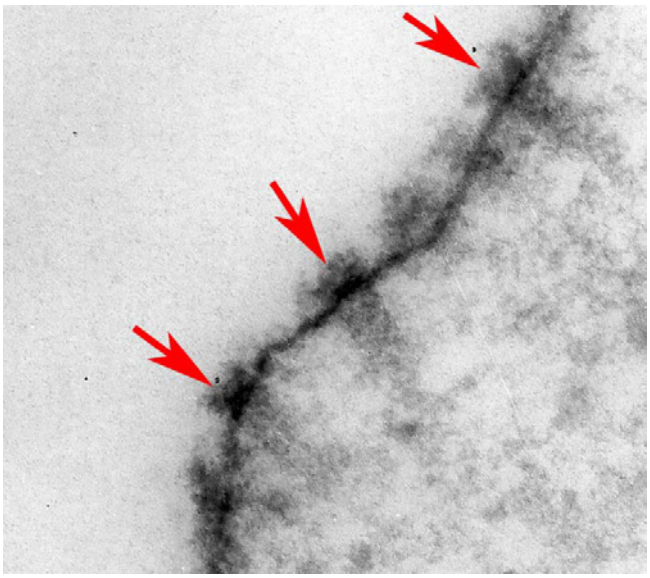

The nuclear routing network revealed with the 1MeV high voltage electron microscopy on 250nm sections

Figure 3b: This oocyte was chemically fixed. It was further processed by embedding, cutting 250 nm thick sections, and staining with uranyl acetate and lead citrate. The image was acquired at the 1MeV HVEM. The arrows point to the entries into the nucleus through the NPCs. Horizontal field width 2030 nm.

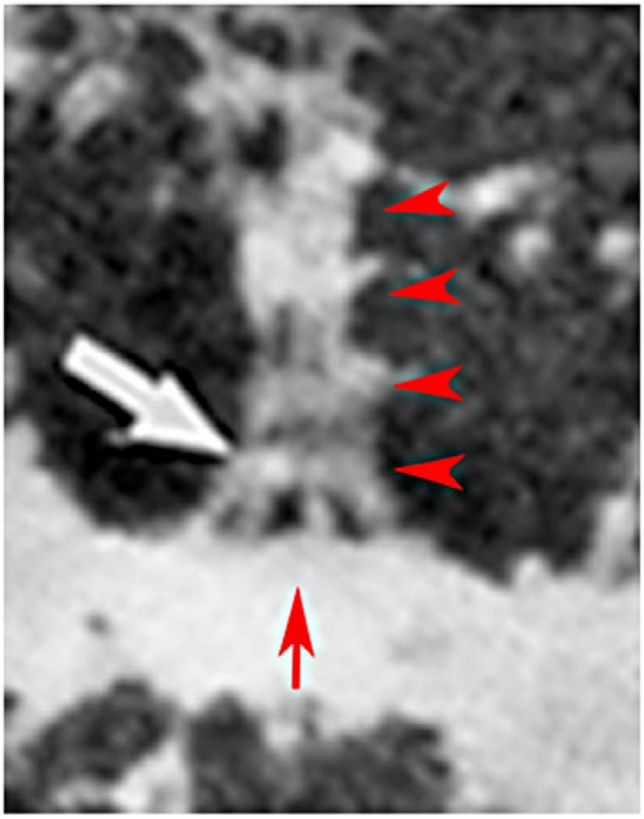

Three-dimensional architecture of the Nuclear Routing Networks (NRNs) revealed by Field Emission Scanning Electron Microscopy (FESEM) on the cross-sections through the nuclear envelope

Figure 4: The oocytes were rapidly cryo-immobilized after microinjection of the transgene vectors, embedded, sectioned perpendicular to the nuclear envelope, de-embedded, and cryo-sputter coated with Pt/C. The entry into the nucleus through the NPC is pointed with the red arrow. The intra-nuclear ring of the NPC basket is pointed with the white arrow. The periodicities along the NRN are pointed with the red arrow heads. Horizontal field width 345 nm.

(ccdsDNA) constructs. For intra-nuclear import, the vectors consisted of the nuclear localization signal (NLS) domain, anti-dsDNA, anti-digoxigenin or anti-biotin domain - anchoring the dsDNA, and chelating domain – harboring Gd, Tb, Eu, Er, Ag, or Au. For nuclear export, the vectors consisted of the nuclear export signal (NES) domain, anti-dsDNA, anti-biotin, and anti-digoxigenin domain anchoring dsDNA plasmids, and metal binding domain coordinating Eu, Er, Gd or Tb. The third and fourth type of the vectors - named shuttle vectors consisted of the NES and NLS domains bioengineered either with the anti-DNA/anti-digoxigenin and Gd chelating domains, or with the anti-biotin/

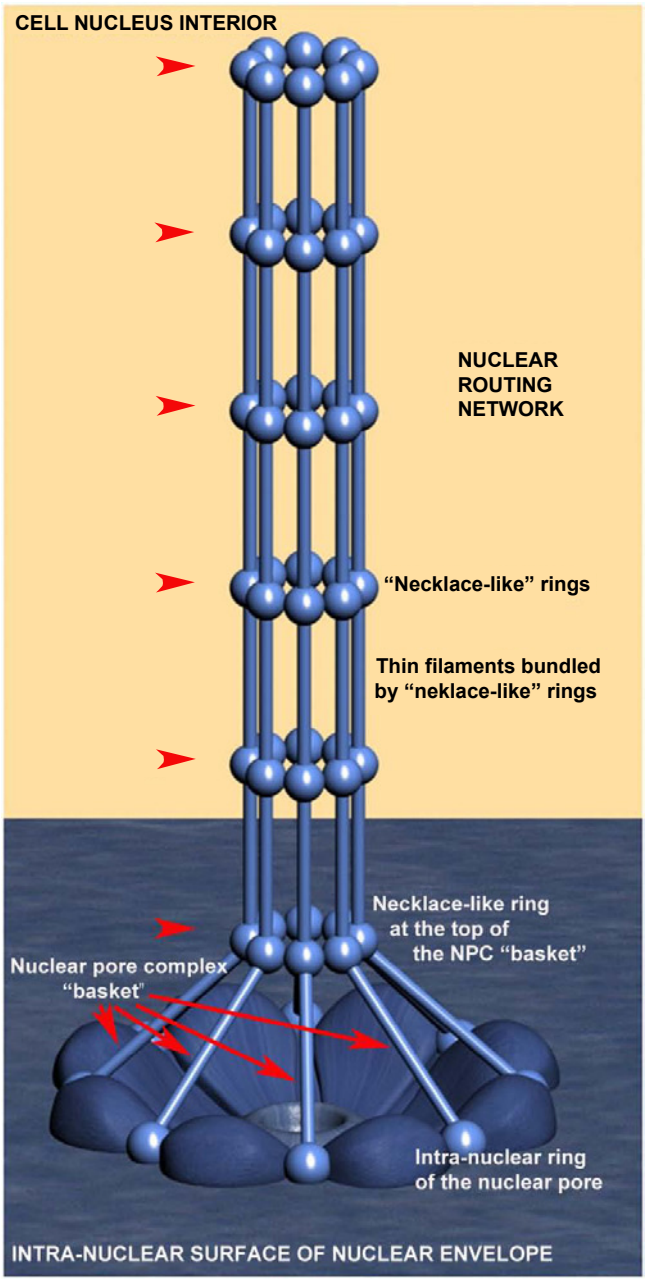

Model of the three-dimensional architecture of the Nuclear Routing Network (NRN)

Figure 5: It illustrates a graphic interpretation of the NRN after the complete removal of chromatin and nucleoplasm. This model was created based upon the data acquired with 3 different techniques of molecular imaging presented in this study.

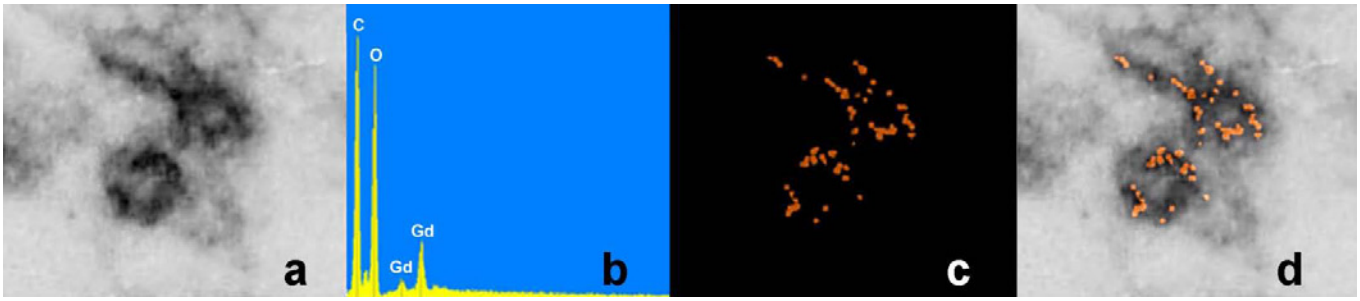

Trafficking of the non-viral, transgene vectors through the NRN revealed by electron energy loss and energy dispersive X-ray spectroscopies

Figure 6a-d: The NLS guided transgene vectors consisting of the scFv (anchoring the closed, circular, double stranded plasmid DNA) and metal binding domain (chelating Gd) were microinjected into the perinuclear space of the oocyte. After 1h, the oocytes were rapidly cryo-immobilized, freeze-substituted, epon embedded, and sectioned. An overview of the NPC and NRN architecture was acquired at zero-loss setting of the EELS on the HB505 FESTEM. (a) The complete elemental spectrum was acquired for every pixel of the scan with the EDXS. This created the elemental spectra database for this scan - the spectrum of one pixel shown as an example (peaks of Gd, C, O are prominent). (b) The spectrum was gated only for Gd and extracted from the complete data base to create the map of the elemental distribution. (c) This elemental map was equivalent to the map of the transgene vectors' distribution. The map of the vectors' distribution (from "c") is overlapped over the architecture of the NPCs and NRNs (from "a") to determine location of the vectors in the oocyte's compartments. (d) Many electron-dense beads were eliminated as the false positive in the TEM, due to the ability to identify the true vectors based upon the elemental map. Horizontal field width in a,c,d 540 nm.

anti-dsDNA/anti-biotin and Eu chelating domains. Microinjections of these vectors into oocytes helped to probe the functions of the nucleo-cytoplasmic transport. At different time intervals passing from the moment of microinjections, the oocytes were cryo-immobilized, stored in liquid nitrogen until processing for molecular imaging with EELS and EDXS. Alternatively, the microinjected oocytes were separated into the fractions: total nucleoplasm, nuclear envelope including the NRNs and NPCs, total cytoplasm for detection with fluorometry or surface plasmon resonance. This procedure prevented any translocations of labeled molecules and/or antibodies during preparation for analysis. Moreover, it assured live-like architecture. Finally, it protected the samples during processing for and imaging.

Analysis of the transgenes' trafficking through various oocytes compartments was pursued in a few steps as illustrated in the figure 6. First, the structural overview at the zero energy loss edge by contrast tuning was acquired (a). Second, the elemental spectrum profile was acquired for every pixel of the image to create the elemental composition data bank (b). Third, a map of Gd distribution in the sample was extracted from the elemental composition data bank (c). Since the Gd atoms were chelated within the dedicated domains of the transgenes' vector, and then the Gd distribution map was indicative of the distribution of the vectors. Fourth, superimposing the Gd map from "c" over the cell structure from "a" revealed distribution of the vectors within the cell structures (d). This approach eliminates false positive identification of the electron-dense particles as transgenes as it may happen in transmission electron microscopy (TEM) and of the strong secondary electron emitters in the scanning electron microscopy (SEM). It also eliminates missed - as false negative, poorly stained transgenes. After outlining areas of the oocyte compartments on the computer screen, the vectors containing Gd atoms were automatically calculated by the elemental analysis software ceiled at 10M counts. The data from ten experiments for each of the transgenes were measured and averaged, the standard deviations calculated and normalized as the ratios between three main compartments: intra-nuclear, nuclear envelope associated structures (NPC + NRN), peri-nuclear. The results are presented in the figures 7-10. The outcome of the intra-nuclear injections of the transgenes guided by the NES is shown in the figure 7. The concentrations of the transgenes inside the nuclei were initially rapidly decreasing, which was followed by less rapid pace until the complete depletion. The concentrations of the transgenes exported outside the nucleus were steadily increasing. These transgenes were initially absent from the NRN and NPCs, but shortly after the microinjections they started to increase, while passing through the NRNs and NPCs. The results of the cytoplasmic injections of the trangenes guided by the NLS are illustrated in the figure 8. The concentrations of the transgenes in the cytoplasm were initially rapidly decreasing, which was followed by less rapid pace until the complete depletion. The concentrations of the transgenes imported into the nucleus were steadily increasing. The passage of the NLS guided transgenes through the NRN had the profile similar to that shown by the NES guided transgenes. This also was indicative of the wave of the exported vectors passing through the NRN. The trafficking profiles of the shuttle vectors guided by the NLS and NES, which were injected into the perinuclear cytoplasmic or intranuclear spaces, were characterized by the initial gradual increase of the concentrations within the NPCs and NRNs. However, within approximately 30 minutes, the concentrations in the NPCs and NRNs reached plateau. This was indicative of the saturation of the NRNs' transporting capabilities. Microinjections of the vectors, which were modified with both the NLS and NES resulted in the initial increase of the concentration in the NRN and NPC fractions. This was indicative of the vectors shuttled back and forth.

Nucleoplasmin, histones, tRNA, and mRNA were used as the most established internal biocompatibility reference tests [52,53]. Import of nucleoplasmin (Np), which was modified with biotin or digoxigenin followed by tagging chelating scFv and injected into the oocytes' cytoplasm is shown in the figure 10. It was trafficking exactly as the native nucleoplasmin shown described previously [52]. Within minutes after microinjection, the Np was already passing through the NPCs and NRNs. Within hours, it entirely cleared from the cytoplasm. Export of tRNA, which was transcribed to incorporate biotin GTP followed by tagging chelating scFv and injected into the oocytes' nuclei, is shown in the figure 9. As in the earlier reports, tRNA swiftly moved into the cytoplasm. It appeared within the NRNs and NPCs within minutes. It entirely cleared from the nucleoplasm within hours.

Altogether, the data acquired in these experiments provide the evidence that, the filamentous bundles, which originate at the NPCs and create complex three-dimensional networks of nano-tubes inside the oocyte nuclei, function as the transporters of the molecules. Therefore, we named them nuclear routing networks (NRNs).

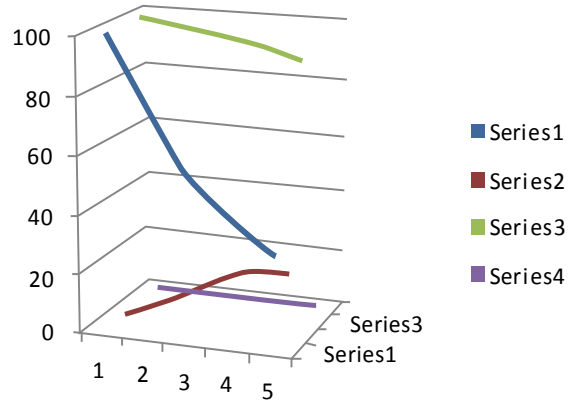

Export of the NES-modified transgenes' vectors after intranuclear microinjections

Figure 7: The NES-modified transgenes' vectors were microinjected into the oocyte nuclei. Every 45 minutes from the time of microinjections, the oocytes were rapidly cryo-immobilized, processed, and analyzed as in the figure 6. The concentrations were measured and normalized against the counts at the zero time as 100%. Series 1 - counts of the NES-modified vectors present in the oocyte nucleus. Series 2 - counts for the vectors in the NRNs and NPCs. Series 3 - counts of the vectors without modification with the NES present in the oocyte nucleus. Series 4 - counts for the non-NES-modified vectors in the NRNs and NPCs. The concentration in the intranuclear space was rapidly falling after microinjections. The concentration in the NPCs and NRNs showed the gradual increase, which followed by the reduction indicative of the passage of the vectors through the NRNs. The concentrations of the transgene vectors were constantly increasing outside of the nuclei as the result of the constant export of the vectors driven by the NES. The concentrations of the vectors which were not modified with the NES gradually reduced due to diffusion, but they did not appear in the NRN and NPC or cytoplasm.

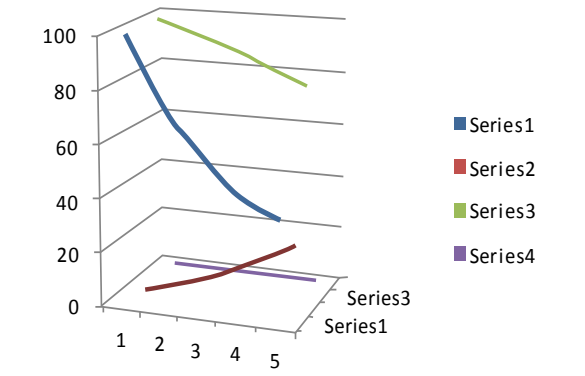

Import of the NLS-modified transgenes' vectors after cytoplasmic microinjections

Figure 8: The cytoplasm of the oocytes was microinjected with the NLS-modified transgenes' vectors. The oocytes were cryo-immobilized and analyzed as in the figure 7. Series 1 - counts of the NLS-modified vectors present in the oocyte cytoplasm. Series 2 - counts for the vectors imported from the cytoplasm into the NRNs and NPCs. Series 3 - counts in the cytoplasm of the vectors, which were not modified with NLS. Series 4 - counts in the NRNs and NPCs of the non-modified vectors. The vectors' concentration in the perinuclear area of cytoplasm was gradually falling, while the concentration in the NRN and NPCs was increasing. This was indicative of the vectors' entry on the route to the nucleoplasm. The concentrations of the vectors which were not modified with the NLS gradually reduced in the cytoplasm, but they did not appear in the NRN and NPC.

Discussion

We revealed the NRN by means of the most advanced molecular imaging techniques [30,52]. The first technique, time-resolved with

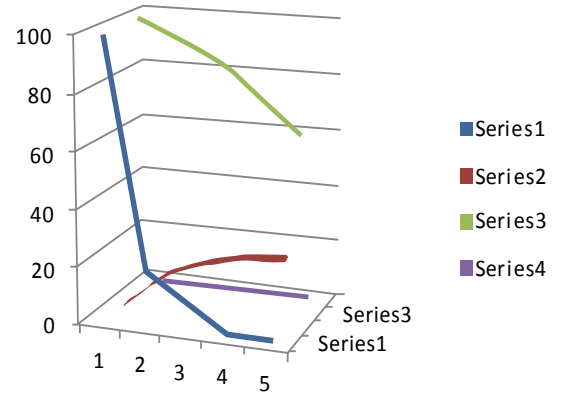

Export of tRNA after intranuclear microinjections

Figure 9: The tRNAs were microinjected into the oocyte nuclei. The oocytes were cryo-immobilized and analyzed at the same time intervals as in the figure 7. The concentrations were measured and normalized against the counts at the zero time as 100%. Series 1 - counts of the tRNA measured in the oocytes nucleus. Series 2 - counts for the tRNA in the NRNs and NPCs. Series 3 - counts of the control RNA measured in a unit volume in the oocyte nucleus. Series 4 - counts of the control RNA in the NRNs and NPCs. The concentration in the intranuclear space was falling after microinjections, while the concentration in the NRN and NPCs gradually increased with the increased passage. The concentrations of the tRNA in the cytoplasm were constantly increasing. The concentration in the intranuclear space was falling after microinjections, while the concentration in the NRN and NPCs gradually increased with the increased passage. The concentrations of the tRNA in the cytoplasm were constantly increasing.

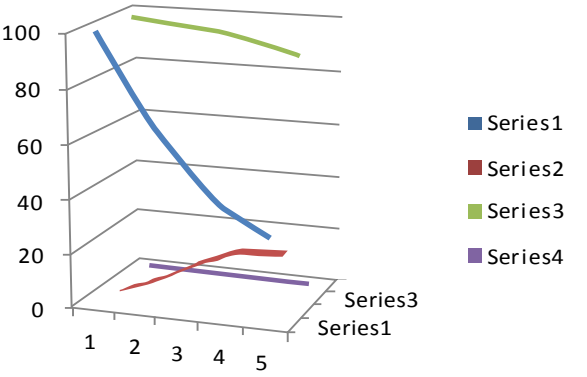

Import of nucleoplasmin after cytoplasmic microinjections

Figure 10: The nucleoplasmin modified with reporters was microinjected into the oocytes' cytoplasm. The oocytes were cryo-immobilized and analyzed at the same time intervals as in the figure 7. Series 1 – counts of the nucleoplasmin present in the oocyte cytoplasm. Series 2 – counts for the nucleoplasmin in the NRNs and NPCs. Series 3 - counts of the core Np present in the oocyte cytoplasm as the control. Series 4 - counts of the core Np present in the NRNs and NPCs as the control. The concentrations of the Np in the cytoplasm were falling after microinjections, but almost did not change in the absence of the NLS. The concentrations of the Np in the NRN and NPCs gradually increased with the increased passage, but were entirely absent for the core Np.

millisecond resolution, rapid cryo-immobilization retained the NPCs and associated structures in their native state. They were not distorted or degraded during preparation for imaging. The second, EELS and EDXS facilitated unequivocal identification of the labeled molecules with the genetically engineered scFv at the supramolecular level of resolution 3D architecture, what was not possible before. Moreover, these imaging modes facilitated imaging of the entire NPCs and NRNs contained within thick sections or whole mounts, which was not possible before. Moreover, thinness of sections and limited depth of field of high

resolution microscopes used in previous studies could not capture the complex architecture of the NRNs. The third, biomolecular engineering of the biocompatible molecules and transgene vectors, modified with the NLS and NES, as well as tagged with the exogenous elements (Gd, Eu, Tb, Er, Ag, Au) helped to reveal their transport through the NRN.

We revealed the NRN in oocytes of *Xenopus laevis*. However, considering the conserved nature of the nuclear pore transport and based upon our works on the human cancer and germ cells, we hypothesize, that the NRN is universal for all eukaryotic cells [52-60]. This may lead to explaining the data reported by other authors. For example, Human Immune-Deficiency Viruses (HIV) in the nuclei of human T lymphocytes moved along the well defined tracks [47]. Similarly, during infecting human lymphoma cells Epstein-Barr virus, the viral RNA did not diffuse uniformly through the nucleus, but occurred in curvilinear tracks between the nuclear center and the NPCs [48]. Their pathways resembled geometries of the NRNs. Hypotheses can be raised, that perhaps the viruses moved along the NRNs to the preferred locations within the nuclei. As another example, the nup140 kDa phosphoproteins, that shuttle between the nucleolus and the cytoplasm, which were tagged with gold beads for TEM, were arraigned into single tracks, heading towards the NPCs [40]. Hypotheses can be raised, that these phosphoproteins moved along the NRNs. As another example, the movements of Poly (A) + RNA, from the sites of transcription to the NPCs in mammalian cell cultures showed that the mRNAs did not diffuse randomly inside the nuclei, but rather were arranged in narrow ribbons [41,43]. Hypotheses can be raised, that the NRNs could be their guiding systems.

This work creates foundation for identifying the molecular components of the NRNs. Clearly, short filaments, projecting from tops of the NPCs, as shown in the earlier publications, can now be considered to be elements of the NRN, which were damaged during the preparations [31, 34, 37]. Nevertheless, those short filaments were identified to contain Nup153, Trp. Moreover, the labels suggesting presence of Trp analogs in the interchromatin spaces were shown [44]. Moreover, nucleoporins were shown to bind to distinct loci of the genome [61,62]. Therefore, the NRNs could serve as the speed-ways between the NPCs and genes' *loci* on chromosomes. Thus, these data suggest the significant role of the NPCs and NRNs they may play in the regulation of gene expression, which is the subject of our currently ongoing works.

All these data suggest a distinct possibility that the NRN exists as a very ergonomically organized distribution system, which efficiently delivers specific molecules to targeted sites within chromosomes. This may be in accord with the hypothesis of the chromosomal domains [45,46]. Identification of the checkpoints and signals within the NRN would be essential for our ability of targeting the therapeutic molecules to the desired destinations inside the nuclei. It would also be essential for controlling accessing of gDNA by mutagenic factors inflicting genetic errors. Futuristically thinking, it would facilitate genomic nanosurgery, i.e., excising disease carrying mutations and inserting the healthy genes, as well as genomic prevention, i.e., introducing molecular safeguards into the transporting mechanisms of the nuclei. Despite the great progress in high throughput genomics and proteomics of the NPCs, elucidation of the functional structure of the NRNs (unlike the very symmetrical NPCs) will most likely be attained by laborious identification of their individual molecular components within the three-dimensional architecture of these macromolecular assemblies *in situ*.

Conflict of interest

The authors declare no conflict of interest.

Acknowledgments

This work was supported by the grants 9420056, 9522771, 9902020, and 0094016 from the NSF, the RR570 grant from the NCRR NIH, the perpetual funds from the PBMEF, and the RR231 grant from the NCRR NIH. The work was pursued at the NIH National Biotechnology Resource, the NIH Nuclear Magnetic Resonance Facility, the UCSD Molecular Imaging Laboratory, the PBMEF, and the SDSU Functional Genomics Center. Technical assistance by J. Dahlke, C. Dodivenaka, J. Haig, A. Hsu, S. Nagel, S. Sanchez, L. Truong, and L. Wohlwend is thankfully acknowledged. Bioinformatics and computer modeling by Michael Malecki are gratefully appreciated. Discussions with Dr. T. Allen, Dr. U. Aebi, Dr. M. Anderson, Dr. D. Bazett-Jones, Dr. J.Dahlberg, Dr. D. Forbes, Dr. M. Hilldreth, Dr. M. Kloc, Dr. E. Lund, Dr. J. Markley, Dr. H. Ris, Dr. D. Spector, Dr. A. Sumner and Dr. W. Szybalski are sincerely appreciated.

References

1. Jamali T, Jamali Y, Mehrbod M, Mofrad MR (2011)Nuclear pore complex: biochemistry and biophysics of nucleocytoplasmic transport in health and disease. Int Rev Cell Mol Biol 287: 233-286.
2. Chatel G, Desai SH, Mattheyses AL, Powers MA, Fahrenkrog B (2012) Domain topology of nucleoporin Nup98 within the nuclear pore complex. J Struct Biol 177: 81-89
3. Löschberger A, van de Linde S, Dabauvalle MC, Rieger B, Heilemann M, et al. (2012) Super-resolution imaging visualizes the eightfold symmetry of gp210 proteins around the nuclear pore complex and resolves the central channel with nanometer resolution. J Cell Sci 125: 570-575.
4. Major AT, Whiley PA, Loveland KL (2011) Expression of nucleocytoplasmic transport machinery: clues to regulation of spermatogenic development. Biochim Biophys Acta 1813: 1668-1688.
5. Funasaka T, Wong RW (2011) The role of nuclear pore complex in tumor microenvironment and metastasis. Cancer Metastasis Rev 30: 239-251.
6. Cohen S, Au S, Panté N (2011) How viruses access the nucleus. Biochim Biophys Acta 1813: 1634-1645.
7. Takeda E, Murakami T, Matsuda G, Murakami H, Zako T, Maeda M, et al. (2011) Nuclear exportin receptor CAS regulates the NPI-1-mediated nuclear import of HIV-1 Vpr. PLoS One 6: e27815.
8. D'Angelo MA, Gomez-Cavazos JS, Mei A, Lackner DH, Hetzer MW (2012) A change in nuclear pore complex composition regulates cell differentiation. Dev Cell 22: 446-458.
9. Grünwald D, Singer RH, Rout M (2011) Nuclear export dynamics of RNA-protein complexes. Nature 475: 333-341.
10. Puente XS, Pinyol M, Quesada V, Conde L, Ordóñez GR, et al. (2011) Whole-genome sequencing identifies recurrent mutations in chronic lymphocytic leukaemia. Nature 475: 101-105.
11. Turner JG, Dawson J, Sullivan DM (2012) Nuclear export of proteins and drug resistance in cancer. Biochem Pharmacol 83: 1021-1032.
12. Nagel J, Groß B, Meggendorfer M, Preiss C, Grez M, et al. (2012) Stably integrated and expressed retroviral sequences can influence nuclear location and chromatin condensation of the integration locus. Chromosoma.
13. Navin N, Hicks J (2011) Future medical applications of single-cell sequencing in cancer. Genome Med 3: 31.
14. Malecki M, Szybalski W (2012) Isolation of single, intact chromosomes from single, selected ovarian cancer cells for in situ hybridization and sequencing. Gene 493: 132-139.
15. Xu X, Hou Y, Yin X, Bao L, Tang A, et al. (2012) Single-cell exome sequencing reveals single-nucleotide mutation characteristics of a kidney tumor. Cell 148: 886-895.
16. Mathews TJ, MacDorman MF (2010) Infant mortality statistics from the 2006 period linked birth/infant death data set. National Vital Statistics Reports 58: 1-32.
17. Copeland GE, Kirby RS (2007) Using birth defects registry data to evaluate infant and childhood mortality associated with birth defects: an alternative to traditional mortality assessment using underlying cause of death statistics. Birth Defects Res A Clin Mol Teratol 79: 792-797.
18. Pennington KP, Swisher EM (2012) Hereditary ovarian cancer: beyond the usual suspects. Gynecol Oncol 124: 347-353.

19. Vollebergh MA, Jonkers J, Linn SC (2012) Genomic instability in breast and ovarian cancers: translation into clinical predictive biomarkers. Cell Mol Life Sci 69: 223-245.

20. Scriven PN, Ogilvie CM, Khalaf Y (2012) Embryo selection in IVF: is polar body array comparative genomic hybridization accurate enough? Hum Reprod 27: 951-953.

21. Musters AM, Repping S, Korevaar JC, Mastenbroek S, Limpens J, et al. (2011) Pregnancy outcome after preimplantation genetic screening or natural conception in couples with unexplained recurrent miscarriage: a systematic review of the best available evidence. Fertil Steril 95: 2153-2157.

22. Dan S, Chen F, Choy KW, Jiang F, Lin J, et al. (2012) Prenatal detection of aneuploidy and imbalanced chromosomal arrangements by massively parallel sequencing. PLoS One 7: e27835.

23. Bianchi DW (2011) Gene expression analysis of amniotic fluid: new biomarkers and novel antenatal treatments. Clin Biochem 44: 448-450.

24. Wang N, Zheng YM, Li L, Jin F (2010) Preimplantation genetic screening: an effective testing for infertile and repeated miscarriage patients? Obstet Gynecol Int 2010: 120130.

25. McCabe LL, McCabe ER (2011) Down syndrome: coercion and eugenics. Genet Med 13: 708-710.

26. Cooray S, Howe SJ, Thrasher AJ (2012) Retrovirus and lentivirus vector design and methods of cell conditioning. Methods Enzymol 507: 29-57.

27. Malecki M, Malecki R (2008) Ovarian cancer suicide gene therapy. Proc SD Acad Sci 87: 249-260.

28. Nowrouzi A, Glimm H, von Kalle C, Schmidt M (2011) Retroviral vectors: post entry events and genomic alterations. Viruses 3: 429-455.

29. Fawcett DW (1966) On the occurrence of a fibrous lamina on the inner aspect of the nuclear envelope in certain cells of vertebrates. Am J Anat 119: 129-145.

30. Malecki M (1991) High voltage electron microscopy and low voltage scanning electron microscopy of human neoplastic cell culture. Scanning Microsc Suppl 5: S53-73.

31. Franke WW, Scheer U, Krohne G, Jarasch ED (1991) The nuclear envelope and the architecture of the nuclear periphery. J Cell Biol 2: 39s-50s.

32. Malecki M, Ris H (1992) Surface topography and intracellular organization of human cells in suspension as revealed by scanning electron microscopy. Scanning 14: 76-85.

33. Ris H, Malecki M (1993) High-resolution field emission scanning electron microscope imaging of internal cell structures after Epon extraction from sections: a new approach to correlative ultrastructural and immunocytochemical studies. J Struct Biol 111: 148-157.

34. Strambio-de-Castillia C, Blobel G, Rout MP (1999) Proteins connecting the nuclear pore complex with the nuclear interior. J Cell Biol 144: 839-855.

35. Kiseleva E, Drummond SP, Goldberg MW, Rutherford SA, Allen TD, et al. (2004) Actin- and protein-4.1-containing filaments link nuclear pore complexes to subnuclear organelles in Xenopus oocyte nuclei. J Cell Sci 117: 2481-2490.

36. Kosova B, Pante N, Rollenhagen C, Podtelejnikov A, Mann M, et al. (2000) Mlp2p, a component of nuclear pore attached intranuclear filaments, associates with nic96p. J Biol Chem 275: 343-350.

37. Cordes VC, Reidenbach S, Köhler A, Stuurman N, van Driel R, et al. (1993) Intranuclear filaments containing a nuclear pore complex protein. J Cell Biol 123: 1333-1344.

38. Wan KM, Nickerson JA, Krockmalnic G, Penman S (1999) The nuclear matrix prepared by amine modification. Proc Natl Acad Sci U S A 96: 933-938.

39. Goldberg MW, Allen TD (1996) The nuclear pore complex and lamina: three-dimensional structures and interactions determined by field emission in-lens scanning electron microscopy. J Mol Biol 257: 848-865.

40. Meier UT, Blobel G (1992) Nopp140 shuttles on tracks between nucleolus and cytoplasm. Cell 70: 127-138.

41. Lawrence JB, Singer RH, Marselle LM (1989) Highly localized tracks of specific transcripts within interphase nuclei visualized by in situ hybridization. Cell 57: 493-502.

42. Murti KG, Brown PS, Ratner L, Garcia JV (1993) Highly localized tracks of human immunodeficiency virus type 1 Nef in the nucleus of cells of a human CD4+ T-cell line. Proc Natl Acad Sci U S A 90: 11895-11899.

43. Huang S, Deerinck TJ, Ellisman MH, Spector DL (1997) The dynamic organization of the perinucleolar compartment in the cell nucleus. J Cell Biol 137: 965-974.

44. Zimowska G, Aris JP, Paddy MR (1997) A Drosophila Tpr protein homolog is localized both in the extrachromosomal channel network and to nuclear pore complexes. J Cell Sci 110: 927-944.

45. Cremer T, Cremer C (2001) Chromosome territories, nuclear architecture and gene regulation in mammalian cells. Nat Rev Genet 2: 292-301.

46. Markaki Y, Gunkel M, Schermelleh L, Beichmanis S et al. (2010) Functional nuclear organization of transcription and DNA replication: a topographical marriage between chromatin domains and the interchromatin compartment. Cold Spring Harb Symp Quant Biol 75: 475-492.

47. Ahmed K, Dehghani H, Rugg-Gunn P, Fussner E, Rossant J, et al. (2010) Global chromatin architecture reflects pluripotency and lineage commitment in the early mouse embryo. PLoS One 5: e10531.

48. Jakel S, Albig W, Kutay U, Bischoff FR, Schwamborn K, et al. (1999) The importin beta/importin 7 heterodimer is a functional nuclear import receptor for histone H1. EMBOJ 18: 2411-2423.

49. Wohlwend D, Strasser A, Dickmanns A, Doenecke D, Ficner R (2007) Thermodynamic analysis of H1 nuclear import: receptor tuning of importinbeta/importin7. J Biol Chem 282: 10707-10719.

50. Capelson M, Liang Y, Schulte R, Mair W, Wagner U, Hetzer MW (2010) Chromatin-bound nuclear pore components regulate gene expression in higher eukaryotes. Cell 140: 372-383.

51. Malecki M, Pietruszkiewicz J (2006) Nanosurgery of cancer with the aid of intracellular, nanoengineered antibodies against antioxidative enzymes. Euro J of Surg Onc 32: S19.

52. Dingwall C. Laskey RA (1986) Protein import into the cell nucleus. Annu Rev Cell Biol 2: 367-390.

53. Feldherr CM, Kallenbach E, Schultz N (1984) Movement of a karyophilic protein through the nuclear pores of oocytes. J Cell Biol 99: 2216-2222.

54. Dahlberg JE, Lund E. Semin (1997) Coupling of nuclear RNA export and protein import in vertebrate cells. Cell Dev Biol 8: 65-70.

55. Dworetzky SI, Feldherr CM (1988) Translocation of RNA-coated gold particles through the nuclear pores of oocytes. The J Cell Biol 106: 575-584.

56. Jarmolowski A, Boelens WC, Izaurralde E, Mattaj IW (1994) Nuclear export of different classes of RNA is mediated by specific factors. J Cell Biol 124: 627-635.

57. Kalderon D, Richardson WD, Markham AF, Smith AE (1984) Sequence requirements for nuclear location of simian virus 40 large-T antigen. Nature 311: 33-38.

58. Lanford RE, Kanda R, Kennedy RC (1986) Induction of nuclear transport with a synthetic peptide homologous to the SV40 T antigen transport signal. Cell 46: 575-582.

59. Dworetzky SI, Lanford RE, Feldherr CM (1988) The effects of variations in the number and sequence of targeting signals on nuclear uptake. J Cell Biol 107: 1279-1287.

60. Ullman KS, Shah S, Powers MA, Forbes DJ (1999) The nucleoporin nup153 plays a critical role in multiple types of nuclear export. Mol Biol Cell 10: 649-664.

61. D'Angelo MA, Gomez-Cavazos JS, Mei A, Lackner DH, Hetzer MW (2012) A change in nuclear pore complex composition regulates cell differentiation. Dev Cell 22: 446-458.

62. Sarma NJ, Buford TD, Haley T, Barbara-Haley K, Santangelo GM, et al. (2011) The nuclear pore complex mediates binding of the Mig1 repressor to target promoters. PLoS One 6: e27117.

63. Malecki M, Hsu A, Truong L, Sanchez S (2002) Molecular immunolabeling with recombinant single-chain variable fragment (scFv) antibodies designed with metal-binding domains. Proc Natl Acad Sci U S A 99: 213-218.